BuildingNet: Learning to Label 3D Buildings

Pratheba Selvaraju[1] Mohamed Nabail[1] Marios Loizou[2] Maria Maslioukova[2]
Melinos Averkiou[2] Andreas Andreou[2] Siddhartha Chaudhuri[3] Evangelos Kalogerakis[1]
[1]UMass Amherst [2]University of Cyprus / CYENS CoE Cyprus [3]Adobe Research / IIT Bombay

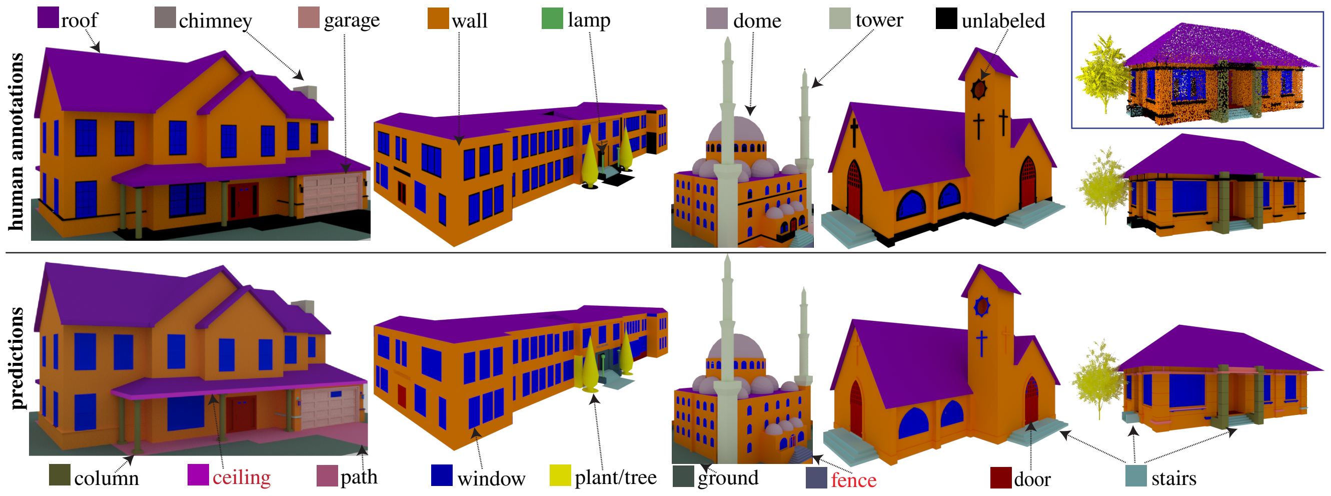

Figure 1: We introduce a dataset of 3D building meshes with annotated exteriors (top). We also present a graph neural network that processes building meshes and labels them by encoding structural and spatial relations between mesh components (bottom). Our dataset also includes a point cloud track (blue box). Examples of erroneous network outputs are in red text.

Abstract

We introduce BuildingNet: (a) a large-scale dataset of 3D building models whose exteriors are consistently labeled, and (b) a graph neural network that labels building meshes by analyzing spatial and structural relations of their geometric primitives. To create our dataset, we used crowdsourcing combined with expert guidance, resulting in $513K$ *annotated mesh primitives, grouped into* $292K$ *semantic part components across* $2K$ *building models. The dataset covers several building categories, such as houses, churches, skyscrapers, town halls, libraries, and castles. We include a benchmark for evaluating mesh and point cloud labeling. Buildings have more challenging structural complexity compared to objects in existing benchmarks (e.g., ShapeNet, PartNet), thus, we hope that our dataset can nurture the development of algorithms that are able to cope with such large-scale geometric data for both vision and graphics tasks e.g., 3D semantic segmentation, part-based generative models, correspondences, texturing, and analysis of point cloud data acquired from real-world buildings. Finally, we show that our mesh-based graph neural network significantly improves performance over several baselines for labeling 3D meshes. Our project page* `www.buildingnet.org` *includes our dataset and code.*

1. Introduction

Architecture is a significant application area of 3D vision. There is a rich body of research on autonomous perception of buildings, led in large part by digital map developers seeking rich annotations and 3D viewing capabilities for building exteriors [15], as well as roboticists who design robots to operate in building interiors (e.g. [46]). Recent advances in AR/VR also rely on computer-aided building analysis [7]. Early work on digital techniques for architectural design, including freeform design explorations as well as full-fledged constructions [16], led to the current ubiquity of computational design tools in architectural studios. In addition, computers can automate the processing of architectural data such as photographs, satellite images and building plans, for archival and analytical purposes (e.g. [63, 33]).

Thus, there is significant incentive to apply modern data-driven geometry processing to the analysis of buildings. However, while buildings are bona fide geometric objects with well-established design principles and clear ontologies, their structural and stylistic complexity is typically greater than, or at least markedly *different from*, those of shapes in common 3D datasets like ShapeNet [6] and ScanNet [11]. This makes them challenging for standard shape analysis pipelines, both for discriminative tasks such as classification, segmentation and point correspondences, as well as for generative tasks like synthesis and style transfer. Further, data-driven methods demand data, and to the best of our knowledge there are no large-scale, consistently-annotated, public datasets of 3D building models.

In this paper, we present BuildingNet, the first publicly available large-scale dataset of annotated 3D building models whose exteriors and surroundings are consistently labeled. The dataset provides 513K annotated mesh primitives across 2K building models. We include a benchmark for mesh and point cloud labeling, and evaluate several mesh and point cloud labeling networks. These methods were developed primarily for smaller single objects or interior scenes and are less successful on architectural data.

In addition, we introduce a graph neural network (GNN) that labels building meshes by analyzing spatial and structural relations of their geometric primitives. Our GNN treats each subgroup as a node, and takes advantage of relations, such as adjacency and containment, between pairs of nodes. Neural message passing in the graph yields the final mesh labeling. Our experiments show that this approach yields significantly better results for 3D building data than prior methods. To summarize, our contributions are:

- The first large-scale, publicly available 3D building dataset with annotated parts covering several common categories, in addition to a benchmark.
- A graph neural network that leverages pre-existing noisy subgroups in mesh files to achieve state-of-the-art results in labeling building meshes.
- An annotation interface and crowdsourcing pipeline for collecting labeled parts of 3D meshes, which could also extend to other categories of 3D data.

2. Related Work

3D shape semantic segmentation datasets. Existing datasets and benchmarks for 3D shape semantic segmentation are limited to objects with relatively simple structure and small number of parts [8, 22, 19, 59, 37, 62]. The earliest such benchmark [8, 22] had 380 objects with few labeled parts per shape. More recently, Uy et al. [53] released a benchmark with 15K scanned objects but focuses on object classification, with part-level segmentations provided only for chairs. The most recent and largest semantic shape segmentation benchmark of PartNet [62] contains $27K$ objects in 24 categories, such as furniture, tools, and household items. However, even with PartNet's fine-grained segmentation, its categories still have a few tens of labeled parts on average. Our paper introduces a dataset for part labeling of 3D buildings, pushing semantic segmentation to much larger-scale objects with more challenging structure and several tens to hundreds of parts per shape.

3D indoor scene datasets. Another related line of work has introduced datasets with object-level annotations in real-world or synthetic 3D indoor environments [20, 1, 40, 47, 5, 11, 29, 64, 14]. In contrast, our dataset focuses on building exteriors, a rather under-investigated domain with its own challenges. While an indoor scene is made of objects, which are often well-separated or have little contact with each other (excluding floors/walls), a building exterior is more like a coherent assembly of parts (windows, doors, roofs) i.e., a single large shape with multiple connected parts, including surroundings (e.g., landscape). Building exteriors share challenges of single-shape segmentation (i.e., segment parts with clean boundaries along contact areas) as well as scene segmentation (i.e., deal with the large-scale nature of 3D data). Buildings also come in a variety of sizes, part geometry and style [32], making this domain challenging for both shape analysis and synthesis.

3D urban datasets. With the explosion of autonomous driving applications, large-scale 3D point cloud datasets capturing urban environments have appeared [39, 17, 44, 2, 49]. These datasets include labels such as roads, vehicles, and sidewalks. Buildings are labeled as a single, whole object. Our dataset contains annotations of building parts, which has its own challenges, as discussed above. The RueMonge14 dataset contains 3D building frontal facades captured from a street in Paris with 8 labels related to buildings [43]. Our buildings are instead complete 3D models with significantly more challenging diversity in geometry, style, function, and with more fine-grained part labels.

Deep nets for 3D mesh understanding. A few recent neural architectures have been proposed for processing meshes. Some network directly operate on the mesh geometric or topological features [34, 18, 27, 45], spectral domain [3, 38, 61, 42], while others transfer representations learned by other networks operating, e.g., on mesh views or voxels [21, 56, 26]. Our method is complementary to these approaches. It is specifically designed to process meshes with pre-existing structure in the form of mesh components (groups of triangles), which are particularly common in 3D building models. CRFs and various grouping strategies with heuristic criteria have been proposed to aggregate such components into labeled parts [56]. Our method instead uses a GNN to label components by encoding spatial and structural relations between them in an end-to-end manner. From this aspect, our method is also related to approaches that place objects in indoor scenes using GNNs operating on bounding box object representations with simple spatial relations, [65, 54], and GNN approaches for indoor scene parsing based on graphs defined over point clusters [28]. Our GNN instead aims to label mesh components represented by rich geometric features, and captures spatial and structural relations specific to building exteriors.

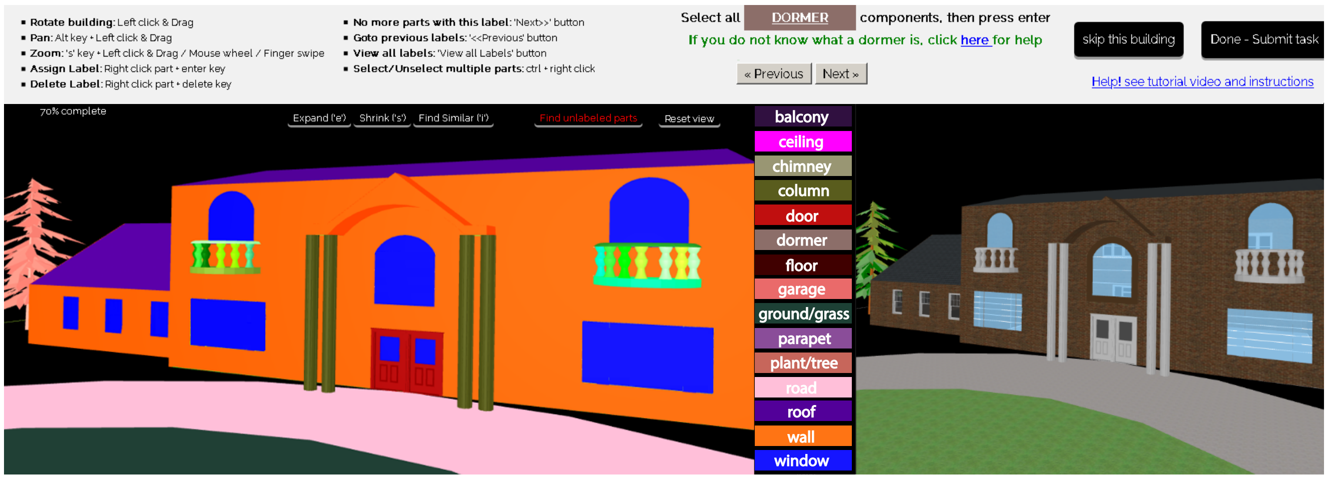

- **Rotate building**: Left click & Drag
- **Pan**: Alt key + Left click & Drag
- **Zoom**: 's' key + Left click & Drag / Mouse wheel / Finger swipe
- **Assign Label**: Right click part + enter key
- **Delete Label**: Right click part + delete key

- **No more parts with this label**: 'Next>>' button
- **Goto previous labels**: '<<Previous' button
- **View all labels**: 'View all Labels' button
- **Select/Unselect multiple parts**: ctrl + right click

Select all DORMER components, then press enter

If you do not know what a dormer is, click here for help

Figure 2: Our interface for labeling 3D building models. The colors of annotated components follow the legend in the middle (we show here a subset of labels - the UI contained 16 more labels in a more extended layout). Any components that have not been labeled so far are shown in shades of light yellow/green (e.g., balcony components). The UI displays instructions on top and offers functionality to facilitate labeling, such as automatic detection of repeated components ("find similar"), automatic grouping/un-grouping of components ("expand"/"shrink"), and auto-focusing on unlabeled ones ("find unlabeled parts").

3D Building Mesh Segmentation and Labeling. There has been relatively little work in this area. Early approaches for semantic segmentation of buildings relied on shallow pipelines with hand-engineered point descriptors and rules [50, 51]. A combinatorial algorithm that groups faces into non-labeled components spanning the mesh with high repetition was proposed in [12]. A user-assisted segmentation algorithm was proposed in [13]. Symmetry has been proposed as a useful cue to group architectural components [25, 36]. Our method instead aims to label 3D building meshes with a learning-based approach based on modern deep backbones for extracting point descriptors. It also incorporates repetitions as a cue for consistent labeling, along with several other geometric and structural cues.

3. Building Data Annotation

We first discuss the procedure we followed to annotate 3D building models. In contrast to 3D models of small and mid-scale objects, such as tools, furniture, and vehicles encountered in existing 3D shape segmentation benchmarks, such as ShapeNet [59, 60] and PartNet [37], buildings tend to contain much richer structure, as indicated by their mesh metadata. For example, one common type of metadata are groupings of polygon faces, commonly known as *mesh subgroups* [37], which correspond to geometric primitives and modeling operations used by modelers while designing shapes. These subgroups often correspond to "pieces" of semantic parts e.g., a window is made of subgroups representing individual horizontal and vertical frame pieces or glass parts. The average number of mesh subgroups per object at the last level of group hierarchy in the largest shape segmentation benchmark (PartNet [37]) is 24.4, and the median is 11. In our dataset, the average number of mesh subgroups per building is 25.5x larger (623.6 subgroups), while the median is 44x larger (497.5 subgroups). We note that these numbers include only building exteriors i.e., without considering building interiors (e.g, indoor furniture). PartNet relied on mesh subgroups for faster annotation i.e., the annotators were manually clicking and grouping them into parts. Selecting each individual mesh subgroup in our case would be too laborious in the case of a large-scale 3D building dataset. To this end, we developed a user interface (UI) that followed the PartNet's principles of well-defined and consistent labelings, yet its primary focus was to deal with the annotation of a massive number of mesh subgroups per building. In particular, our UI offers annotators the option of *label propagation* to similar subgroups based on both geometric and mesh metadata to enable faster labeling. Another focus was to achieve *consensus* across several trained crowdworkers annotating in parallel. To this end, we employed a majority voting process. We focused on crowdsourcing annotations for *common part labels* encountered in buildings. In the rest of this section, we describe our user interface (UI) for interactive labeling of 3D buildings (Section 3.1), and the dataset collection process (Section 3.2).

3.1. Interface for labeling

Our interface is shown in Figure 2. On the left window, we display the building with a distinct color assigned to each mesh subgroup. When a subgroup is annotated, it changes color from the default palette (shades of light green and yellow) to a predetermined, different color according to its label. On the right, we display the textured version of the building so that crowdworkers also access color cues useful for labeling. The workers have full 3D control of viewpoint (pan, zoom, rotate). Changes on the viewpoint are reflected in both windows. On the top of the interface, we provide instructions and links with examples of parts from real-world buildings for each label. The workers are asked to label the mesh subgroups through a sequence of questions e.g., “label all walls”, then “label all windows”, and so on. Alternatively, they can skip the questions, and directly select a desired part label from the list appearing in the middle of the UI. To perform an assignment of a currently selected label to a mesh subgroup, the workers simply right-click on it and press enter. Alternatively, they can select multiple subgroups and annotate them altogether. All adjacent subgroups with the same label are automatically merged into a single labeled *component* to decrease the workload of manual merging. We note that we considered the possibility of incorporating mesh cutting tools to split large subgroups into smaller ones for assigning different labels, as done in PartNet [37]. However, such tools require reconstruction into watertight meshes, which could not be achieved for most building subgroups due to their non-manifold geometry, disconnected or overlapping faces, and open mesh boundaries. For the majority of buildings in our dataset, we observed that each subgroup can be assigned with a single part label without requiring further splits. Annotators were also instructed not to label any (rare) subgroups that contained parts with different labels.

Clicking individual mesh subgroups for assigning part labels can be still cumbersome, since buildings have hundreds or thousands of them. Our UI takes advantage of the fact that buildings often have repeated mesh subgroups e.g., the same window mesh is re-used multiple times in a facade during 3D modeling. Thus, in a pre-processing step, we found all duplicate mesh subgroups by checking if they have the same mesh connectivity (mesh graph) and vertex locations match after factoring out rigid transformations. Details about duplicate detection are provided in the supplementary material. Workers are then given the option to select all subgroup duplicates and propagate the same label to all of them at once, as shown in Figure 3(top). Another UI feature was to allow users to “expand” a mesh subgroup selection by taking advantage of any hierarchical grouping metadata. This expansion was performed by iteratively moving one level up in the mesh group hierarchy and finding all subgroups sharing the same parent with the initially selected subgroup, as shown in Figure 3(bottom). We refer readers to our supplementary video showing a tutorial with details of our UI operations.

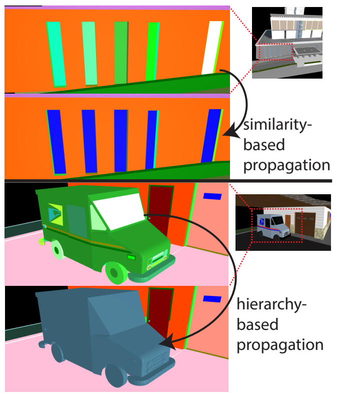

Figure 3: Label propagation to repeated subgroups *(top)* or their parents *(bottom)*. Initially selected subgroup is in white.

Table 1: Statistics per building category. *From left to right*: building category, total number of models, average/median/minimum/maximum number of mesh subgroups per model, average number of unique subgroups.

Category	num# models	avg# subgrps	med# subgrps	min# subgrps	max# subgrps	avg# un. subgrps
Residential	1,424	678.7	547	83	1989	167.1
Commercial	153	723.4	606	90	1981	159.8
Religious	540	487.0	348	93	1981	139.9
Civic	67	628.8	480	118	1822	144.4
Castles	85	609.8	485	125	1786	193.0
Whole Set	2,000	623.6	497.5	83	1989	160.5

3.2. Dataset and Benchmark

To create our dataset, we mined building models from the 3D Warehouse repository [52]. Mining was driven by various quality checks e.g., excluding low-poly, incomplete, untextured meshes, and meshes with no or too few subgroups. We also categorized them into basic classes following the Wikipedia’s article on “list of building types” [58] and an Amazon MTurk questionnaire. Since we aimed to gather annotations of building exteriors, during a pre-processing step we removed interior structure from each building. This was done by performing exhaustive ray casting originating from mesh faces of each subgroup and checking if the rays were blocked. We also used ray casting to orient faces such that their normals are pointing outwards [48]. Details about mining, classifying, and pre-processing of the 3D models are given in our supplement.

Part labels. To determine a set of *common* labels required in our UI to annotate building exteriors, we launched an initial user study involving a small subset of 100 buildings across all classes and 10 participants with domain expertise (graduate students in civil engineering and architecture). For this study, we created a variant of our UI asking users to explicitly type tags for mesh subgroups. We selected a list of 31 frequently entered tags to define our label set (see Table 2 and Appendix B of our supplement for details).

Annotation procedure. One possibility to annotate building parts would be to hire “professionals” (e.g., architects). Finding tens or hundreds of such professionals would be extremely challenging and costly in terms of time and resources. In an early attempt to do so, we found that consistency was still hard to achieve without additional verification steps and majority voting. On the other hand, hiring non-skilled, non-trained crowdworkers would have the disadvantage of gathering erroneous annotations. We instead proceeded with a more selective approach, where we identified crowdworkers after verifying their ability to conduct the annotation task reliably based on our provided tutorial and instructions. During our worker qualification stage, we released our UI on MTurk accessible to any worker interested in performing the task. After a video tutorial, including a web page presenting real-world examples of parts per label, the workers were asked to label a building randomly selected from a predetermined pool of buildings with diverse structure and part labels. We then checked their labelings, and qualified those workers whose labeling was consistent with our instructions. We manually verified the quality of their annotations. Out of $2,520$ participants, 342 workers qualified. After this stage, we released our dataset only to qualified MTurkers. We asked them to label as many parts as they can with a tiered compensation to encourage more labeled area (ranging from \$0.5 for labeling minimum 70% of the building area to \$1.0 for labeling $> 90\%$). Out of the 342 qualified MTurkers, 168 accepted to perform the task in this phase. Each qualified MTurker annotated $\sim$60 buildings and each annotation took $\sim$19.5min on average.

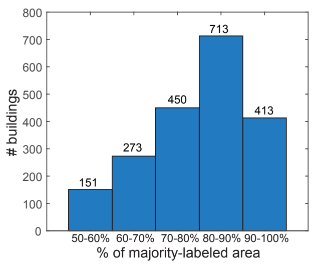

Dataset. We gathered annotations for 2K buildings. Each building was annotated by 5 different, qualified MTurkers (10K annotations in total). We accepted a label for each subgroup if a majority of at least 3 MTurkers out of 5 agreed on it. The inlet figure shows a histogram displaying the distribution of buildings (vertical axis) for different bins of percentage of surface area labeled with achieved majority (horizontal axis). All buildings in our dataset have labeled area more than 50%, and most have $> 80\%$ area labeled. In terms of annotator consistency, i.e., the percentage of times that the subgroup label selected by a qualified MTurker agreed with the majority, we found that it is 92.0%, indicating that the workers were highly consistent. Our resulting 2K dataset has $513,087$ annotated mesh subgroups, and $291,998$ annotated components (after merging adjacent subgroups with the same label). The number of unique annotated subgroups and components are $111,832$ and $86,492$ respectively. Table 9 presents subgroup statistics for each basic building category. Table 2 shows labeled component statistics per part label. We include more statistics in the supplement.

Splits. We split our dataset into 1600 buildings for training, 200 for validation, 200 for testing ($80/10/10\%$ proportion). The dataset has no duplicate buildings. We created the splits such that (a) the distribution of building classes and parts is similar across the splits (Table 2 and supplementary) and (b) test buildings have high majority-labeled area ($> 85\%$) i.e., more complete labelings for evaluation.

Table 2: Number of labeled components per part label in our dataset, along with their number and frequency in the training split, hold-out validation, and test split.

Label	# labeled comp.	# in training split (%)	# in validation split (%)	# in test split (%)
Window	140,972	109,218 (47.8%)	15,740 (55.1%)	16,014 (46.0%)
Plant	26,735	20,974 (9.2%)	1,870 (6.5%)	3,891 (11.2%)
Wall	22,814	18,468 (8.1%)	2,270 (7.9%)	2,076 (6.0%)
Roof	12,881	10,342 (4.5%)	1,396 (4.9%)	1,143 (3.3%)
Banister	13,954	9,678 (4.2%)	1,467 (5.1%)	2,809 (8.1%)
Vehicle	8,491	7,421 (3.2%)	716 (2.5%)	354 (1.0%)
Door	9,417	7,363 (3.2%)	785 (2.7%)	1,269 (3.6%)
Fence	5,932	5,637 (2.5%)	88 (0.3%)	207 (0.6%)
Furniture	6,282	5,000 (2.2%)	575 (2.0%)	707 (2.0%)
Column	6,394	4,870 (2.1%)	623 (2.2%)	901 (2.6%)
Beam	6,391	4,814 (2.1%)	437 (1.5%)	1,140 (3.3%)
Tower	4,478	3,873 (1.7%)	286 (1.0%)	319 (0.9%)
Stairs	4,193	2,960 (1.3%)	472 (1.7%)	761 (2.2%)
Shutters	2,275	1,908 (0.8%)	77 (0.3%)	290 (0.8%)
Ground	2,057	1,572 (0.7%)	229 (0.8%)	256 (0.7%)
Garage	1,984	1,552 (0.7%)	182 (0.6%)	250 (0.7%)
Parapet	1,986	1,457 (0.6%)	153 (0.5%)	376 (1.1%)
Balcony	1,847	1,442 (0.6%)	199 (0.7%)	206 (0.6%)
Floor	1,670	1,257 (0.5%)	205 (0.7%)	208 (0.6%)
Buttress	1,590	1,230 (0.5%)	53 (0.2%)	307 (0.9%)
Dome	1,327	1,098 (0.5%)	114 (0.4%)	115 (0.3%)
Path	1,257	1,008 (0.4%)	113 (0.4%)	136 (0.4%)
Ceiling	1,193	903 (0.4%)	111 (0.4%)	179 (0.5%)
Chimney	1,090	800 (0.4%)	103 (0.4%)	187 (0.5%)
Gate	827	737 (0.3%)	65 (0.2%)	25 (0.1%)
Lighting	921	702 (0.3%)	51 (0.2%)	168 (0.5%)
Dormer	798	601 (0.3%)	48 (0.2%)	149 (0.4%)
Pool	742	544 (0.2%)	78 (0.3%)	120 (0.3%)
Road	590	444 (0.2%)	55 (0.2%)	91 (0.3%)
Arch	524	393 (0.2%)	11 (0.03%)	120 (0.3%)
Awning	386	295 (0.1%)	19 (0.1%)	72 (0.2%)
Total	291,998	228,561	28,591	34,846

Tracks. We provide two tracks in our benchmark. In the first track, called "BuildingNet-Mesh", algorithms can access the mesh data, including subgroups. In this aspect, they can take advantage of any pre-existing mesh structure common in 3D building models. The algorithms are evaluated in two conditions: when the RGB texture is available, and when it is not. In the second condition, algorithms must label the building using only geometric information. The second track, called "BuildingNet-Points", is designed for large-scale point-based processing algorithms that must deal with unstructured point cloud data without access to mesh structure or subgroups, which is still challenging even in the noiseless setting. To this end, for each mesh, we sample $100K$ points with Poisson disc sampling, to achieve a near-uniform sampling similarly to PartNet [37]. The point normals originate from triangles. There are also two evaluation conditions: with and without RGB color for points.

4. Building GNN

We now describe a graph neural network for labeling 3D meshes by taking advantage of pre-existing mesh structure in the form of subgroups. The main idea of the network is to take into account spatial and structural relations between subgroups to promote more coherent mesh labeling. The input to our network is a 3D building mesh with subgroups $\mathcal{C} = \{c_i\}_{i=1}^{N}$, where N is the number of subgroups, and the output is a label per subgroup. In the next section, we describe how the graph representing a building is created, then we discuss our GNN architecture operating on this graph.

Graph Nodes. For each 3D building model, we create a node for each mesh subgroup. Nodes carry an initial raw representation of the subgroup. Specifically, we first sample the mesh with 100K points (same point set used in the "BuildingNet-Points" track), then process them through the 3D sparse convolutional architecture of Minkowski network (MinkowskiUNet34 variant [9]). We also experimented using PointNet++ [41]. We extract per-point features from the last layer of these nets, then perform average pooling over the points originating from the faces of the subgroup to extract an initial node representation. We concatenate this representation with the 3D barycenter position of the subgroup, its mesh surface area, and the coordinates of the opposite corners of its Oriented Bounding Box (OBB) so that we capture its spatial dimensions explicitly. The combination of the above features in the resulting 41D node representation $\mathbf{n}_i$ yielded better performance in our experiments.

Proximity edges. Driven by the observation that nearby subgroups tend to have the same label (e.g., adjacent pieces of glass or frame are labeled as "window"), or related labels (e.g., windows are often adjacent to walls), we create edges for pairs of subgroups that capture their degree of proximity. To avoid creating an overly dense graph, which would pose excessive memory overheads for the GNN, we created edges for pairs of subgroups whose distance was up to 10% of the average of their OBB diagonals. Relaxing this bound did not improve results. To avoid a hard dependency on a single threshold, and to capture the degree of subgroup proximity at multiple scales, we computed the percentage of point samples of each subgroup whose distance to the other subgroup is less than 1%, 2.5%, 5%, and 10% of the average of their OBB diagonals. Given a pair of subgroups (c_i, c_j), this results in a $4D$ edge raw representation $\mathbf{e}_{i,j}^{(prox)}$, where each entry approximates the surface area percentage of c_i proximal to c_j at a different scale. Similarly, we compute a $4D$ representation $\mathbf{e}_{j,i}^{(prox)}$ for the opposite edge direction.

Support edges. Certain arrangements of labels are often expected along the upright axis of the building e.g., the roof is on top of walls. We create a "supporting" edge for each subgroup found to support another subgroup, and "supported-by" edges of opposite direction for each subgroup found to be supported by another subgroup. The edges are created by examining OBB spatial relations. Specifically, as in the case of proximity edges, we compute a multi-scale 4D edge raw representation $\mathbf{e}_{i,j}^{(ontop)}$ measuring the area percentage of c_i's bottom OBB face lying above the c_j's top OBB face for different distances 1%, 2.5%, 5%, 10% of the average of the two OBB's heights. We also compute a 4D edge raw representation $\mathbf{e}_{j,i}^{(below)}$ corresponding to the the surface area percentage of c_j's top OBB face lying beneath the c_i's bottom OBB face.

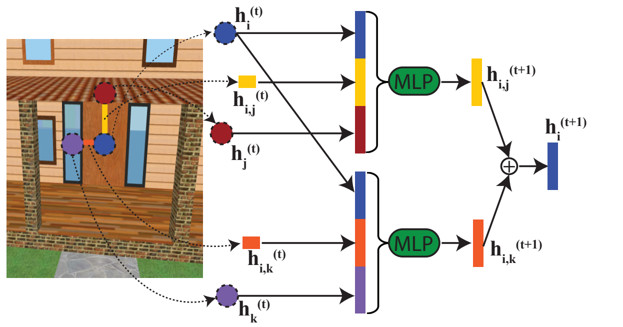

Figure 4: Architecture of the message passing layer. The door representation (blue node) is updated from a support edge (yellow edge) to a roof component (red node) and a proximity edge (orange edge) to a window (purple node).

Similarity edges. Subgroups placed under a symmetric arrangement often share the same label (e.g., repeated windows along a facade). We create an edge per pair of subgroups capturing repetition. For each pair of subgroups, we compute the bidirectional Chamfer distance between their sample points after rigid alignment. To promote robustness to any minor misalignment, or small geometric differences between subgroups, we create similarity edges if the Chamfer distance $d_{i,j}$ is less than 10% of the average of their OBB diagonals. Increasing this bound did not improve results. We normalize it within $[0, 1]$, where 1.0 corresponds to the above upper bound, and use $\mathbf{e}_{i,j}^{(symm)} = 1 - d_{i,j}$ as raw similarity edge representation. We also use the same representation for this opposite direction: $\mathbf{e}_{j,i}^{(symm)} = \mathbf{e}_{i,j}^{(symm)}$.

Containment edges. Driven by the observation that parts, such as doors or windows, are enclosed by, or contained within other larger parts, such as walls, we create edges for pairs of subgroups capturing their degree of containment. For each pair of subgroups, we measure the amount of c_i's volume contained within the c_j's OBB and also their volume Intersection over Union as a 2D edge representation $\mathbf{e}_{i,j}^{(contain)}$ (and similarly for the opposite edge direction).

Network architecture. The network updates node and edge representations at each layer inspired by neural message passing [24]. Figure 4 shows one such layer of message passing. Below we explain our architecture at test time.

Initialization. Given a pair of subgroups c_i and c_j, we first concatenate their edge representations across all types:

$$\mathbf{e}_{i,j} = \{\mathbf{e}_{i,j}^{(prox)}, \mathbf{e}_{i,j}^{(ontop)}, \mathbf{e}_{i,j}^{(below)}, \mathbf{e}_{i,j}^{(contain)}, \mathbf{e}_{i,j}^{(sim)}\}$$

We note that some of the edge types might not be present between two subgroups based on our graph construction. The entries of our edge representations indicate degree of proximity, support, containment, or similarity, and are normalized between $[0,1]$ by definition. Zero values for an edge representation of a particular type indicate non-existence for this type. Each raw edge representation $\mathbf{e}_{i,j}$ is initially processed by a MLP to output a learned representation $\mathbf{h}_{i,j}^{(0)} = MLP\big(\mathbf{e}_{i,j};\mathbf{w}^{(0)}\big)$, where $\mathbf{w}^{(0)}$ are learned MLP parameters. The initial node representation is $\mathbf{h}_i^{(0)} = \mathbf{n}_i$.

Node and edge updates. Each of the following layers process the node and edge representations of the previous layer through MLPs and mean aggregation respectively:

$$\mathbf{h}_{i,j}^{(l+1)} = MLP\big(\mathbf{h}_i^{(l)},\mathbf{h}_j^{(l)},\mathbf{h}_{i,j}^{(l)};\mathbf{w}^{(l)}\big)$$
$$\mathbf{h}_i^{(l+1)} = \frac{1}{|N(i)|}\sum_{j\in\mathcal{N}(i)} \mathbf{h}_{i,j}^{(l+1)}$$

where $\mathbf{w}^{(l)}$ are learned MLP parameters. We use 3 layers of node/edge updates. Finally, the last GNN layer processes the node representations of the third layer, and decodes them to a probability per label using a MLP and softmax. Details about the architecture are in the supplement.

Training loss. Since some parts are more rare than others, as shown in Table 2, we use a weighted softmax loss to train our network, where weights are higher for rarer parts to promote correct labeling for them (i.e., higher mean Part IoU). For each building, the loss is $L = -\sum_{c_i\in\mathcal{L}} w_l \cdot \hat{\mathbf{q}}_i \log \mathbf{q}_i$, where $\mathcal{L}$ is the set of all annotated subgroups in the building, $\hat{\mathbf{q}}_i$ is the ground-truth one-hot label vector for subgroup c_i, $\mathbf{q}_i$ is its predicted label probabilities, and w_l is the weight for the label empirically set to be the log of inverse label frequency (i.e., a smoothed version of inverse frequency weights similarly to [35]). We use the same loss to train the MinkowskiNet used in our node representation: the loss is simply applied to points instead of subgroups. We experimented with other losses, such as the focal loss [30] and the class-balanced loss [10], but we did not find significant improvements in our dataset (see supplementary material).

Implementation details. Training of the BuildingGNN is done through the Adam optimizer [23] with learning rate 0.0001, beta coefficients are $(0.9, 0.999)$ and weight decay is set to 10^{-5}. We pick the best model and hyper-parameters based on the performance in the holdout validation split.

5. Results

We now discuss our evaluation protocol, then show qualitative and quantitative results for our benchmark tracks.

Evaluation protocol. Since most part classes are commonly encountered across different building categories (e.g., walls, doors, windows), all evaluated methods are trained across all five building categories (i.e., no category-specific training). Methods must also deal with the part class imbalance of our dataset. For evaluation in the point cloud track ("BuildingNet-Points"), we use the metrics of mean shape IoU and part IoU, as in PartNet [37]. We also report the per-point classification accuracy. For the mesh track ("BuildingNet-Mesh"), the same measures are applied on triangles. However, since triangles may differ in area, we propose the following IoU variations, where the contribution of each triangle is weighted by its face area. Given all the annotated triangles across all buildings of the test dataset T_D, the part IoU for a label l is measured as:

$$IoU(l) = \frac{\sum_{t\in T_D} a_t\cdot([y_t == l]\wedge[\hat{y}_t == l])}{\sum_{t\in T_D} a_t\cdot([y_t == l]\vee[\hat{y}_t == l])}$$

where $\hat{y}_t$ is the majority-annotated (ground-truth) label for a triangle $t\in T_d$, y_t is the predicted label for it, and $[\cdot]$ evaluates the above binary expressions. The shape IoU for a shape s with a set of annotated triangles T_s is measured as:

$$IoU(s) = \frac{1}{|L_s|}\sum_{l\in L_s}\frac{\sum_{t\in T_s} a_t\cdot([y_t == l]\wedge[\hat{y}_t == l])}{\sum_{t\in T_s} a_t\cdot([y_t == l]\vee[\hat{y}_t == l])}$$

where L_s is the set of all labels present in the annotations or predictions for that shape. We also report the per-triangle classification accuracy weighted by face area [22].

"BuildingNet-Points" track. As an initial seed for the leaderboard of this track, we evaluated three popular nets able to handle our $100K$ point sets: PointNet++ [41], MID-FC [55], and MinkowskiUNet34 [9]. We also tried other point-based networks e.g., DGCNN [57], but were unable to handle large point clouds due to excessive memory requirements (see our supplementary material for more discussion). All networks were trained under the same augmentation scheme (12 global rotations per building and small random translations). For all networks, we experimented with SGD, Adam [23], with and without warm restarts [31], and selected the best scheduler and hyperparameters for each of them based on the validation split. We did not use any form of pre-training. Table 3 reports the results. We observe that the MinkowskiNet offers the best performance. We also observe that the inclusion of color tends to improve performance e.g., we observe a 3% increase in Part IoU for MinkowskiNet. Another observation is that compared to PartNet classes, where the Part IoU ranges between $\sim$30 $-$ 70% for PointNet++, the performance in our dataset is much lower: PointNet++ has 14.1% Part IoU. Even for the best performing method (MinkowskiNet), the part IoU is still relatively low (29.9%), indicating that our building dataset is substantially more challenging.

"BuildingNet-Mesh" track. For our mesh track, we first include a number of baselines which rely on networks trained on the point cloud track, then transferring their results to meshes. One strategy for this transfer is to build correspondences between mesh faces and nearest points.

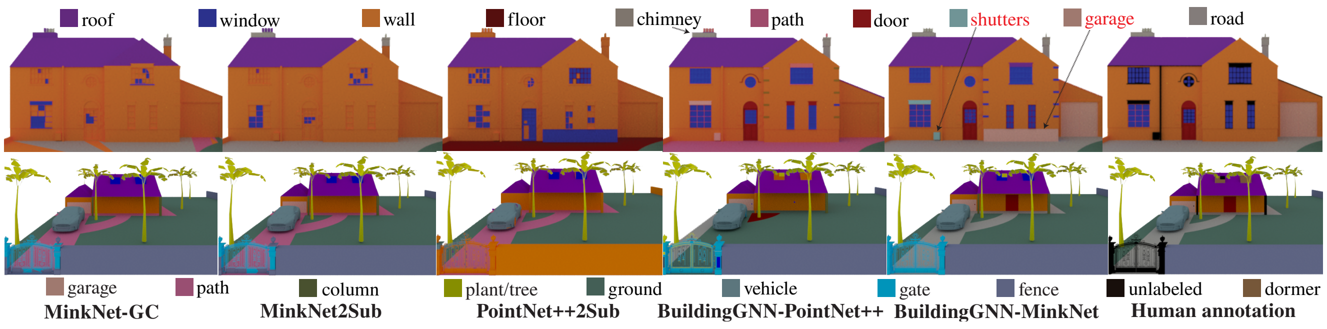

Figure 5: Comparisons with other methods. Despite a few errors (red text), the BuildingGNN is closer to human annotations.

Table 3: "BuildingNet-Point" track results. The column '**n**?' means whether networks use point normals, and the column '**c**?' means whether they use RGB color as input.

Method	**n**?	**c**?	Part IoU	Shape IoU	Class acc.
PointNet++	✓	×	8.8%	12.2%	52.7%
MID-FC(nopre)	✓	×	20.9%	19.0%	59.4%
MinkNet	✓	×	**26.9%**	**22.2%**	**62.2%**
PointNet++	✓	✓	14.1%	16.7%	59.5%
MID-FC(nopre)	✓	✓	25.0%	22.3%	63.2%
MinkNet	✓	✓	**29.9%**	**24.3%**	**65.5%**

Specifically, for each point we find its nearest triangle. Since some triangles might not be associated with any points, we also build the reverse mapping: for each triangle, we find its closest point. In this manner, every triangle t has a set of points P_t assigned to it with the above bi-directional mapping. Then we perform average pooling of the point probabilities per triangle: $\mathbf{q}_t = \sum_{p \in P_t} \mathbf{q}_p / |P_t|$ where $\mathbf{q}_p$ and $\mathbf{q}_t$ are point and triangle probabilities respectively. We report results of these baselines in Table 4. We note that we tried max pooling, yet average pooling had better performance (see supplement). Another strategy is to aggregate predictions based on mesh subgroups instead of triangles i.e., average probabilities of points belonging to each subgroup. This strategy takes advantage of mesh structure and improves results. Another baseline is Graph Cuts (GC) on the mesh, which has been used in mesh segmentation [22] (see supplement for the GC energy). Finally, we report results from our GNN ("BuildingGNN"), using PointNet++ or MinkowskiNet node features. The BuildingGNN significantly improves the respective baselines e.g., with color as input, BuildingGNN with PointNet++ features improves Part IoU by 15.4% over the best PointNet++ variant, while BuildingGNN with MinkowskiNet features improves Part IoU by 5.6% over the best MinkowskiNet variant. The BuildingGNN with MinkowskiNet features performs the best with or without color. Our supplement includes an ablation study showing that each edge type in the BuildingGNN improves performance over using node features alone, while the best model is the one with all edges.

Qualitative results. Figure 5 shows comparisons of BuildingGNN with other methods. We observe that its predictions are closer to human annotations compared to others. Figure 1 presents more results from BuildingGNN.

Table 4: "BuildingNet-Mesh" results. PointNet++2Triangle means triangle-pooling with PointNet++ (similarly for others). PointNet2Sub means subgroup-pooling. MinkNet-GC means graph cuts with MinkowskiUNet34 unary terms.

Method	**n**?	**c**?	Part IoU	Shape IoU	Class acc.
PointNet++2Triangle	✓	×	8.8%	13.1%	54.7%
MidFC2Triangle	✓	×	23.1%	22.1%	42.9%
MinkNet2Triangle	✓	×	28.8%	26.7%	64.8%
PointNet++2Sub	✓	×	9.5%	16.0%	57.9%
MidFC2Sub	✓	×	26.4%	28.4%	46.2%
MinkNet2Sub	✓	×	33.1%	36.0%	69.9%
MinkNet-GC	✓	×	29.9%	28.3%	66.0%
BuildingGNN-PointNet++	✓	×	29.0%	33.5%	67.9%
BuildingGNN-MinkNet	✓	×	**40.0%**	**44.0%**	**74.5%**
PointNet2Triangle	✓	✓	14.0%	18.0%	60.7%
MidFC2Triangle	✓	✓	27.3%	26.2%	45.6%
MinkNet2Triangle	✓	✓	32.8%	29.2%	68.1%
PointNet2Sub	✓	✓	16.1%	23.5%	64.8%
MidFC2Sub	✓	✓	30.3%	33.1%	48.6%
MinkNet2Sub	✓	✓	37.0%	39.1%	73.2%
MinkNet-GC	✓	✓	33.8%	31.1%	68.9%
BuildingGNN-PointNet++	✓	✓	31.5%	35.9%	73.9%
BuildingGNN-MinkNet	✓	✓	**42.6%**	**46.8%**	**77.8%**

6. Discussion

We presented the first large-scale dataset for labeling 3D buildings and a GNN that takes advantage of mesh structure to improve labeling. A future avenue of research is to automatically discover segments in point clouds and embed them into a GNN like ours. Currently, edges are extracted heuristically. Learning edges and features in an end-to-end manner may improve results. Finally, mesh cutting and hierarchical labeling can lead to richer future dataset versions.

Acknowledgements. We thank Rajendra Adiga, George Artopoulos, Anastasia Mattheou, Demetris Nicolaou for their help. Our work was funded by Adobe, NSF (CHS-1617333), the ERDF and the Republic of Cyprus through the RIF (Project EXCELLENCE/1216/0352), and the EU H2020 Research and Innovation Programme and the Republic of Cyprus through the Deputy Ministry of Research, Innovation and Digital Policy (Grant Agreement 739578).

References

[1] I. Armeni, O. Sener, A. R. Zamir, H. Jiang, I. Brilakis, M. Fischer, and S. Savarese. 3D Semantic Parsing of Large-Scale Indoor Spaces. In *Proc. CVPR*, 2016. 2

[2] J. Behley, M. Garbade, A. Milioto, J. Quenzel, S. Behnke, C. Stachniss, and J. Gall. SemanticKITTI: A Dataset for Semantic Scene Understanding of LiDAR Sequences. In *Proc. ICCV*, 2019. 2

[3] Davide Boscaini, Jonathan Masci, Emanuele Rodolà, and Michael Bronstein. Learning shape correspondence with anisotropic convolutional neural networks. In *Proc. NIPS*, 2016. 2

[4] Yuri Boykov, Olga Veksler, and Ramin Zabih. Fast approximate energy minimization via graph cuts. *IEEE Trans. Pat. Ana. & Mach. Int.*, 23(11), 2001. 13

[5] Angel Chang, Angela Dai, Thomas Funkhouser, Maciej Halber, Matthias Niessner, Manolis Savva, Shuran Song, Andy Zeng, and Yinda Zhang. Matterport3D: Learning from RGB-D Data in Indoor Environments. In *Proc. 3DV*, 2017. 2

[6] Angel X. Chang, Thomas Funkhouser, Leonidas Guibas, Pat Hanrahan, Qixing Huang, Zimo Li, Silvio Savarese, Manolis Savva, Shuran Song, Hao Su, Jianxiong Xiao, Li Yi, and Fisher Yu. ShapeNet: An Information-Rich 3D Model Repository. Technical Report arXiv:1512.03012 [cs.GR], Stanford University — Princeton University — Toyota Technological Institute at Chicago, 2015. 1

[7] L. Chen, W. Tang, N. W. John, T. R. Wan, and J. J. Zhang. Context-aware mixed reality: A learning-based framework for semantic-level interaction. *Computer Graphics Forum*, 39(1), 2020. 1

[8] Xiaobai Chen, Aleksey Golovinskiy, and Thomas Funkhouser. A Benchmark for 3D Mesh Segmentation. *ACM Trans. on Graphics*, 28(3), 2009. 2

[9] Christopher Choy, JunYoung Gwak, and Silvio Savarese. 4D Spatio-Temporal ConvNets: Minkowski Convolutional Neural Networks. In *Proc. CVPR*, 2019. 6, 7

[10] Yin Cui, Menglin Jia, Tsung-Yi Lin, Yang Song, and Serge Belongie. Class-Balanced Loss Based on Effective Number of Samples. In *Proc. CVPR*, 2019. 7, 14

[11] Angela Dai, Angel X. Chang, Manolis Savva, Maciej Halber, Thomas Funkhouser, and Matthias Nießner. ScanNet: Richly-annotated 3D Reconstructions of Indoor Scenes. In *Proc. CVPR*, 2017. 2

[12] Ilke Demir, Daniel G. Aliaga, and Bedrich Benes. Coupled Segmentation and Similarity Detection for Architectural Models. *ACM Trans. on Graphics*, 34(4), 2015. 3

[13] I. Demir, D. G. Aliaga, and B. Benes. Procedural Editing of 3D Building Point Clouds. In *Proc. ICCV*, 2015. 3

[14] Huan Fu, Rongfei Jia, Lin Gao, Mingming Gong, Binqiang Zhao, Steve Maybank, and Dacheng Tao. 3D-FUTURE: 3D Furniture shape with TextURE. *arXiv preprint arXiv:2009.09633*, 2020. 2

[15] Google Maps. `https://maps.google.com`, 2017. 1

[16] Jon Arteta Grisaleña. *The Paradigm of Complexity in Architectural and Urban Design (PhD Thesis)*. University of Alcala, 2017. 1

[17] Timo Hackel, N. Savinov, L. Ladicky, Jan D. Wegner, K. Schindler, and M. Pollefeys. SEMANTIC3D.NET: A new large-scale point cloud classification benchmark. In *Proc. ISPRS*, 2017. 2

[18] Rana Hanocka, Amir Hertz, Noa Fish, Raja Giryes, Shachar Fleishman, and Daniel Cohen-Or. MeshCNN: A Network with an Edge. *ACM Trans. on Graphics*, 38(4), 2019. 2

[19] Ruizhen Hu, Lubin Fan, and Ligang Liu. Co-Segmentation of 3D Shapes via Subspace Clustering. *Computer Graphics Forum*, 31(5), 2012. 2

[20] Binh-Son Hua, Quang-Hieu Pham, Duc Thanh Nguyen, Minh-Khoi Tran, Lap-Fai Yu, and Sai-Kit Yeung. SceneNN: A Scene Meshes Dataset with aNNotations. In *Proc. 3DV*, 2016. 2

[21] Evangelos Kalogerakis, Melinos Averkiou, Subhransu Maji, and Siddhartha Chaudhuri. 3D Shape Segmentation with Projective Convolutional Networks. In *Proc. CVPR*, 2017. 2

[22] Evangelos Kalogerakis, Aaron Hertzmann, and Karan Singh. Learning 3D Mesh Segmentation and Labeling. *ACM Trans. on Graphics*, 29(3), 2010. 2, 7, 8, 13

[23] Diederik P. Kingma and Jimmy Ba. Adam: A Method for Stochastic Optimization. In *Proc. ICLR*, 2015. 7

[24] Thomas Kipf, Ethan Fetaya, Kuan-Chieh Wang, Max Welling, and Richard Zemel. Neural Relational Inference for Interacting Systems. In *Proc. ICML*, 2018. 6

[25] N. Kobyshev, H. Riemenschneider, A. Bodis-Szomoru, and L. Van Gool. Architectural decomposition for 3D landmark building understanding. In *Proc. WACV*, 2016. 3

[26] Abhijit Kundu, Xiaoqi Yin, Alireza Fathi, David Ross, Brian Brewington, Thomas Funkhouser, and Caroline Pantofaru. Virtual Multi-view Fusion for 3D Semantic Segmentation. In *Proc. ECCV*, 2020. 2

[27] Alon Lahav and Ayellet Tal. MeshWalker: Deep Mesh Understanding by Random Walks. *ACM Trans. on Graphics (Proc. SIGGRAPH Asia)*, 39(6), 2020. 2

[28] L. Landrieu and M. Simonovsky. Large-Scale Point Cloud Semantic Segmentation with Superpoint Graphs. In *Proc. CVPR*, 2018. 2

[29] Wenbin Li, Sajad Saeedi, John McCormac, Ronald Clark, Dimos Tzoumanikas, Qing Ye, Yuzhong Huang, Rui Tang, and Stefan Leutenegger. InteriorNet: Mega-scale Multi-sensor Photo-realistic Indoor Scenes Dataset. In *Proc. BMVC*, 2018. 2

[30] Tsung-Yi Lin, Priya Goyal, Ross B. Girshick, Kaiming He, and Piotr Dollár. Focal Loss for Dense Object Detection. In *Proc. ICCV*, 2017. 7, 14

[31] I. Loshchilov and F. Hutter. SGDR: Stochastic Gradient Descent with Warm Restarts. In *Proc. ICLR*, 2017. 7

[32] Zhaoliang Lun, Evangelos Kalogerakis, and Alla Sheffer. Elements of Style: Learning Perceptual Shape Style Similarity. *ACM Trans. on Graphics*, 34(4), 2015. 2

[33] Jisan Mahmud, True Price, Akash Bapat, and Jan-Michael Frahm. Boundary-aware 3D building reconstruction from a single overhead image. In *Proc. CVPR*, 2020. 1

[34] Jonathan Masci, Davide Boscaini, Michael Bronstein, and Pierre Vandergheynst. Geodesic convolutional neural networks on Riemannian manifolds. In *Proc. ICCV Workshops*, 2015. 2

[35] Tomas Mikolov, Ilya Sutskever, Kai Chen, Greg Corrado, and Jeffrey Dean. Distributed Representations of Words and Phrases and Their Compositionality. In *Proc. NIPS*, 2013. 7

[36] Niloy J. Mitra, Leonidas J. Guibas, and Mark Pauly. Partial and Approximate Symmetry Detection for 3D Geometry. *ACM Trans. on Graphics*, 25(3), 2006. 3

[37] Kaichun Mo, Shilin Zhu, Angel X. Chang, Li Yi, Subarna Tripathi, Leonidas J. Guibas, and Hao Su. PartNet: A Large-Scale Benchmark for Fine-Grained and Hierarchical Part-Level 3D Object Understanding. In *Proc. CVPR*, 2019. 2, 3, 4, 5, 7

[38] Federico Monti, Davide Boscaini, Jonathan Masci, Emanuele Rodola, Jan Svoboda, and Michael M Bronstein. Geometric deep learning on graphs and manifolds using mixture model cnns. In *Proc. CVPR*, 2017. 2

[39] D. Munoz, J. A. Bagnell, N. Vandapel, and M. Hebert. Contextual classification with functional Max-Margin Markov Networks. In *Proc. CVPR*, 2009. 2

[40] Duc Thanh Nguyen, Binh-Son Hua, Lap-Fai Yu, and Sai-Kit Yeung. A robust 3D-2D interactive tool for scene segmentation and annotation. *IEEE Trans. Vis. & Comp. Graphics*, 24(12), 2018. 2

[41] Charles R Qi, Li Yi, Hao Su, and Leonidas J Guibas. PointNet++: Deep Hierarchical Feature Learning on Point Sets in a Metric Space. In *Proc. NIPS*, 2017. 6, 7

[42] Yi-Ling Qiao, Lin Gao, Jie Yang, Paul L. Rosin, Yu-Kun Lai, and Xilin Chen. Learning on 3D Meshes with Laplacian Encoding and Pooling. *IEEE Trans. Vis. & Comp. Graphics*, 2020. 2

[43] Hayko Riemenschneider, András Bódis-Szomorú, Julien Weissenberg, and Luc Van Gool. Learning Where to Classify in Multi-view Semantic Segmentation. In *Proc. ECCV*, 2014. 2

[44] Xavier Roynard, Jean-Emmanuel Deschaud, and Franois Goulette. Paris-Lille-3D: A large and high-quality ground truth urban point cloud dataset for automatic segmentation and classification. *The International Journal of Robotics Research*, 37(6), 2018. 2

[45] Jonas Schult, Francis Engelmann, Theodora Kontogianni, and Bastian Leibe. DualConvMesh-Net: Joint Geodesic and Euclidean Convolutions on 3D Meshes. In *Proc. CVPR*, 2020. 2

[46] G. Sepulveda, J. C. Niebles, and A. Soto. A Deep Learning Based Behavioral Approach to Indoor Autonomous Navigation. In *Proc. ICRA*, 2018. 1

[47] Shuran Song, Fisher Yu, Andy Zeng, Angel X Chang, Manolis Savva, and Thomas Funkhouser. Semantic Scene Completion from a Single Depth Image. In *Proc. CVPR*, 2017. 2

[48] Kenshi Takayama, Alec Jacobson, Ladislav Kavan, and Olga Sorkine-Hornung. A Simple Method for Correcting Facet Orientations in Polygon Meshes Based on Ray Casting. *Journal of Computer Graphics Techniques (JCGT)*, 3(4), 2014. 4

[49] Weikai Tan, Nannan Qin, Lingfei Ma, Ying Li, Jing Du, Guorong Cai, Ke Yang, and Jonathan Li. Toronto-3D: A Large-scale Mobile LiDAR Dataset for Semantic Segmentation of Urban Roadways. In *Proc. CVPR Workshops*, 2020. 2

[50] Alexander Toshev and Ben Taskar. Detecting and parsing architecture at city scale from range data. In *Proc. CVPR*, 2010. 3

[51] Alexander Toshev and Ben Taskar. 3d all the way: Semantic segmentation of urban scenes from start to end in 3d. In *Proc. CVPR*, 2015. 3

[52] Trimble. *3D Warehouse*, 2020. 4, 11

[53] Mikaela Angelina Uy, Quang-Hieu Pham, Binh-Son Hua, Duc Thanh Nguyen, and Sai-Kit Yeung. Revisiting point cloud classification: A new benchmark dataset and classification model on real-world data. In *Proc. ICCV*, 2019. 2

[54] Kai Wang, Yu-An Lin, Ben Weissmann, Manolis Savva, Angel X. Chang, and Daniel Ritchie. PlanIT: Planning and Instantiating Indoor Scenes with Relation Graph and Spatial Prior Networks. *ACM Trans. on Graphics*, 38(4), 2019. 2

[55] Peng-Shuai Wang, Yu-Qi Yang, Qian-Fang Zou, Zhirong Wu, Yang Liu, and Xin Tong. Unsupervised 3D Learning for Shape Analysis via Multiresolution Instance Discrimination. *ACM Trans. on Graphics*, 2020. 7

[56] Xiaogang Wang, Bin Zhou, Haiyue Fang, Xiaowu Chen, Qinping Zhao, and Kai Xu. Learning to Group and Label Fine-Grained Shape Components. *ACM Trans. on Graphics*, 37(6), 2018. 2

[57] Yue Wang, Yongbin Sun, Ziwei Liu, Sanjay E. Sarma, Michael M. Bronstein, and Justin M. Solomon. Dynamic graph CNN for learning on point clouds. *ACM Trans. on Graphics*, 38(5), 2019. 7, 16

[58] Wikipedia. *List of building types*, 2018. 4, 11

[59] Li Yi, Vladimir G. Kim, Duygu Ceylan, I-Chao Shen, Mengyan Yan, Hao Su, Cewu Lu, Qixing Huang, Alla Sheffer, and Leonidas Guibas. A Scalable Active Framework for Region Annotation in 3D Shape Collections. *ACM Trans. on Graphics*, 35(6), 2016. 2, 3

[60] Li Yi, Lin Shao, Manolis Savva, Haibin Huang, Yang Zhou, Qirui Wang, Benjamin Graham, Martin Engelcke, Roman Klokov, Victor S. Lempitsky, Yuan Gan, Pengyu Wang, Kun Liu, Fenggen Yu, Panpan Shui, Bingyang Hu, Yan Zhang, Yangyan Li, Rui Bu, Mingchao Sun, Wei Wu, Minki Jeong, Jaehoon Choi, Changick Kim, Angom Geetchandra, Narasimha Murthy, Bhargava Ramu, Bharadwaj Manda, M. Ramanathan, Gautam Kumar, P. Preetham, Siddharth Srivastava, Swati Bhugra, Brejesh Lall, Christian Häne, Shubham Tulsiani, Jitendra Malik, Jared Lafer, Ramsey Jones, Siyuan Li, Jie Lu, Shi Jin, Jingyi Yu, Qixing Huang, Evangelos Kalogerakis, Silvio Savarese, Pat Hanrahan, Thomas A. Funkhouser, Hao Su, and Leonidas J. Guibas. Large-Scale 3D Shape Reconstruction and Segmentation from Shapenet Core55. *CoRR*, abs/1710.06104, 2017. 3

[61] Li Yi, Hao Su, Xingwen Guo, and Leonidas J Guibas. SyncSpecCNN: Synchronized spectral cnn for 3D shape segmentation. In *Proc. CVPR*, 2017. 2

[62] Fenggen Yu, Kun Liu, Yan Zhang, Chenyang Zhu, and Kai Xu. PartNet: A Recursive Part Decomposition Network for Fine-Grained and Hierarchical Shape Segmentation. In *Proc. CVPR*, 2019. 2

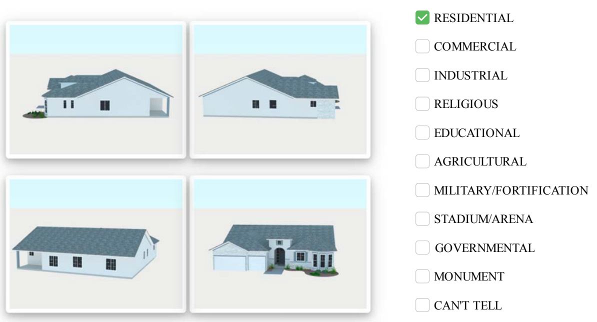

Figure 6: Web questionnaire for classifying a model into basic building categories

[63] Matthias Zeppelzauer, Miroslav Despotovic, Muntaha Sakeena, David Koch, and Mario Döller. Automatic prediction of building age from photographs. In *Proc. ICMR*, 2018. 1

[64] Jia Zheng, Junfei Zhang, Jing Li, Rui Tang, Shenghua Gao, and Zihan Zhou. Structured3D: A Large Photo-realistic Dataset for Structured 3D Modeling. In *Proc. ECCV*, 2020. 2

[65] Yang Zhou, Zachary While, and Evangelos Kalogerakis. SceneGraphNet: Neural Message Passing for 3D Indoor Scene Augmentation. In *Proc. ICCV*, 2019. 2

– Supplementary Material –

Appendix A: Building collection

Mining building models. We used the Trimble 3D Warehouse repository [52] to mine 3D building models. Specifically, we used keywords denoting various building categories, following a snapshot from Wikipedia's article on "list of building types" [58]. The article contained 181 common building types, such as "house", "hotel", "skyscraper", "church", "mosque", "city hall", "castle", "office building", and so on, organized into basic categories, such as residential, commercial, industrial, agricultural, military, religious, educational, and governmental buildings. For each keyword, we retrieved the first $10K$ models. Since some keyword searches returned much fewer buildings, and since identical models were retrieved across different searches (e.g., a building can have both tags "house" and "villa"), we ended up with $48,439$ models. The models were stored in the COLLADA file format.

Mesh-based filtering. Low-poly meshes often represent low-quality or incomplete buildings, and they often cause problems in rendering and geometry processing. Thus, we removed models with less than $3K$ faces and also removed models with extremely large number of faces (more than $1M$ faces) that tend to significantly slow down mesh processing and rendering for interactive segmentation (total $13,628$ models removed). Since our UI relies on labeling mesh subgroups (submeshes) stored in the leaf nodes of the COLLADA hierarchy, we excluded under-segmented models with less than 50 mesh subgroups, and over-segmented models with more than $5K$ mesh subgroups, which would be more challenging to label (total $4,958$ models removed). As a result, the filtered dataset contained $29,853$ models.

Crowdworker-based filtering. The above keyword searches can be affected by noisy metadata, such as erroneous and irrelevant tags not describing the actual shape class. As a result, most of the retrieved models did not represent buildings. Some models also contained entire neighborhoods or multiple buildings. Thus, our next step was to filter 3D models that did not represent single buildings. We resorted to crowdworkers from Amazon Mechanical Turk (MTurk) to verify whether each model is a single building or not, and also classify it into basic categories following Wikipedia's categorization. To this end, we created web questionnaires showing each model from four viewpoints with elevation 0 degrees from the ground plane, and azimuth difference 90^o degrees. We asked MTurk participants (MTurkers) to select a category that best describe the model (see Figure 6 for an example of rendered views, and basic categories we used). We instructed them to answer "can't tell" if the displayed model did not represent a single building, or when they could not recognize it.

Each participant was asked to complete a questionnaire with 20 queries randomly picked from our filtered set of models. Each query showed one model (Figure 6). Queries were shown in a random order. Each query was repeated twice in the questionnaire in a random order to detect unreliable participants providing inconsistent answers (i.e., we had 10 unique queries per questionnaire). We filtered out unreliable MTurk participants who gave two inconsistent answers to more than 3 out of the 10 unique queries in the questionnaire. Each participant was allowed to answer one questionnaire at most to ensure participant diversity. We had total $4,344$ different, reliable MTurk participants in this study. For each of the models, we gathered consistent votes from 7 different MTurk participants. We accepted a building category for a model, if it was voted by at least 5 out of 7 MTurkers. We note that this majority is statistically significant: given 10 categories, the probability of a model getting 5 out of 7 votes given random answers is negligible according to a binomial test ($p < 0.001$). We removed models lacking majority votes (i.e., they were not buildings, or the category could not be determined with high agreement).

The categories "agricultural", "industrial", "stadium" had less than 40 buildings, thus, we decided to exclude them since their part variability and corresponding labels, would not be sufficiently represented in training, validation, and test splits of the segmentation dataset. We also decided to merge the "educational" and "governmental" buildings into a single broader category, called "civic" buildings commonly used to characterize both types of buildings, since we observed that the exterior of a governmental building (e.g., town hall) is often similar to the exterior of an educational one (e.g., public library or college). The remaining number of models characterized as buildings from our study was $2,286$. We note that all models in our dataset are stored as COLLADA files, and have hierarchy tree depth ≥ 2 (excl. the root). We refer the reader to Table 5 for statistics per basic category in our dataset and its splits.

Mesh pre-processing. The meshes in the above dataset were pre-processed to (a) *detect and remove interior structure* for each building (since we aimed to gather annotations of building exteriors), (b) *detect exact duplicates of subgroups* useful for label propagation, as discussed in Section 3.1 (interface for labeling) in our main paper. To detect whether a subgroup is interior, we sample 10 points per each triangle in the subgroup and shoot rays to 50 external viewpoints from all these sample points. If a single ray escapes from the subgroup, it is marked as external, otherwise it is internal. We remove all subgroups marked as internal. For duplicate detection, we process all-pairs of subgroups in a building. Specifically, for each pair of subgroups, we exhaustively search for upright axis rotations minimizing Chamfer distance. The optimal translation is computed from the difference of the vertex location barycenters. After factoring out the rigid transformation, we compute one-to-one vertex correspondences based on closest pairs in Euclidean space. If all closest pairs have distance less than 10^{-6} of the average OBB diagonals of the subgroups, we also check if their mesh connectivity matches i.e., the subgroup mesh adjacency matrix is the same given the corresponding vertices. If they match, the pair is marked as duplicate. Finally, all such pairs are merged into sets containing subgroups found to be duplicates of each other.

Table 5: From left to right: number of models per basic building category after filtering (original buildings), number of buildings whose parts were labeled by crowdworkers in our dataset (labeled buildings), number and percentage of training, hold-out validation and test buildings

Category	#orig. build.	#label. build.	# train. (%)	# val. (%)	# test (%)
Residential	1424	1266	1007 (62.9%)	133 (66.5%)	126 (63.0)%
Commercial	153	131	104 (6.5%)	16 (8.0%)	11 (5.5%)
Religious	540	469	386 (24.1%)	38 (19.0%)	45 (22.5%)
Civic	67	61	45 (2.8%)	8 (4.0%)	8 (4.0%)
Castles	85	73	58 (3.6%)	5 (2.5%)	10 (5.0%)
Total:	2286	2,000	1600 (80%)	200 (10%)	200 (10%)

Appendix B: Part labels

To determine a set of *common* labels used to identify parts in buildings, we created a variant of our UI that asked users to explicitly type tags for selected components instead of selecting labels from a predefined list. We gathered tags from people who have domain expertise in the fields of building construction or design. Specifically, we asked 10 graduate students in civil engineering and architecture to tag components in a set of 100 buildings uniformly distributed across the different categories. Each student labeled 3-10 different buildings. We selected tags that appeared at least in 0.5% of the labeled components to filter out uncommon tags. We concatenated the remaining tags with the most frequent tags appearing in the COLLADA leaf nodes (appearing at least in 0.5% of subgroups). We merged synonyms and similar tags.

The resulting list had 39 tags. During the main phase of annotation of our 2K buildings, 8 tags were used very sparsely: less than 0.05% subgroups throughout the dataset were annotated with these tags: "ramp", "canopy", "tympanum", "crepidoma", "entablature", "pediment", "bridge", and "deck". We decided them to exclude them from our dataset since the number of train or test subgroups with these labels would be too low (less than 10, or they existed in only one building). Any subgroups annotated with these tags were considered as "unlabeled" (undetermined) ones.

Table 6: Statistics regarding mesh resolution in our dataset. From left to right: building category, average/median number of faces and vertices.

Category	avg. # faces	med. # faces	avg. # vertices	med. # vertices
Residential	58,522.7	32,295.5	18,830.6	10,684.0
Commercial	49,248.5	28,862.0	16,722.6	10,041.0
Religious	51,882.7	25,979.0	16,687.4	8,654.0
Civic	40,380.1	20,512.0	13,910.2	7,281.0
Castles	70,731.2	26,493.0	21,050.0	8,822.0
Whole Set	56,250.4	29,741.5	18,120.9	9,845.0

Appendix C: Additional dataset statistics

As discussed in our main paper, we gathered $10,000$ annotations from qualified MTurkers for $2,000$ buildings (5 annotations per building). Table 6 shows statistics on the polygon resolution of the meshes in our 2K dataset. Table 7 reports the worker consistency per part label, which is measured as the percentage of times that a subgroup label selected by a qualified MTurker agrees wit the majority. Table 8 reports the worker consistency per building category for the training, hold-out validation, and test split. We observe that the worker consistency remains similar across all splits and building categories.

Table 9 reports statistics on the number of subgroups per building category, unique subgroups (counting repeated subgroups with exactly the same mesh geometry as one unique subgroup), and number of annotated subgroups. We note that there were often subgroups that represented tiny, obscure pieces (e.g., subgroups with a few triangles covering a tiny area of a wall, beam, or frame), and these were often not labeled by annotators. As we explained in the main paper, most of the buildings had more than 80% of their area labeled (and all had $> 50\%$ labeled area). Table 10 presents more statistics on the labeled components (merged, adjacent subgroups with the same label) of the $2K$ building dataset per each basic category.

Appendix D: Network and experiments details

BuildingGNN. We provide more details about the structure of the BuildingGNN network architecture in Table 11. Table 12 presents statistics on the number of edges per type used in BuildingGNN for our training set.

MinkNet-GC. As mentioned in the experiments section of our main paper, we implemented a simple graph-cuts variant, called MinkNet-GC, that incorporates label probabilities from MinkowskiUNet34 as unary terms, and a pairwise term that depends on angles between triangles, inspired by [22]. Specifically, we use the following energy that we minimize using [4]:

$$E(\boldsymbol{y}) = \sum_{i \in \mathcal{F}} \psi(y_i) + \sum_{i \in \mathcal{F}} \sum_{j \in \mathcal{N}(i)} \phi(y_i, y_j) \qquad (1)$$

where $\boldsymbol{y} = \{y_i\}$ are the label assignments we wish to compute by minimizing the above energy, $\mathcal{F}$ is the set of faces in a mesh, and $\mathcal{N}(i)$ are the adjacent faces of each face i. The unary term is expressed as follows: $\psi(y_i) = -\log f(y_i)$, where $f(y_i)$ is the probability distribution over part labels associated with the face i produced through average pooling of probabilities computed from MinkowskiUNet34 on the triangle's associated points. The pairwise term uses angles between face normals, $\phi'(y_i, y_j) = -\lambda' \cdot \log(\min(\omega_{i,j}/90^o, 1))$, for $y_i \neq y_j$, where $\omega_{i,j}$ is the angle between the normals of faces i, j.

Table 7: Worker consistency for each different part label.

Label	Worker consistency
Window	93.4%
Plant	98.7%
Wall	88.2%
Roof	88.7%
Banister	86.5%
Vehicle	99.2%
Door	84.9%
Fence	85.9%
Furniture	95.1%
Column	87.2%
Beam	76.3%
Tower	81.4%
Stairs	92.0%
Shutters	79.3%
Ground	84.8%
Garage	86.9%
Parapet	82.6%
Balcony	75.9%
Floor	79.1%
Buttress	85.0%
Dome	83.5%
Corridor	70.6%
Ceiling	78.4%
Chimney	93.3%
Gate	90.8%
Lighting	90.9%
Dormer	70.4%
Pool	86.8%
Road	73.8%
Arch	72.1%
Awning	59.5%

Table 8: Worker consistency in the training, hold-out validation, test split, and our whole dataset per category.

Category	Worker Consistency			
	train.	val.	test	all
Residential	92.2%	93.3%	91.5%	92.2%
Commercial	87.7%	89.4%	95.1%	88.6%
Religious	91.4%	91.7%	91.7%	91.5%
Civic	93.6%	98.8%	98.0%	94.9%
Castles	94.1%	88.8%	88.3%	92.9%
Average:	**91.8%**	**92.4%**	**92.9%**	**92.0%**

Table 9: Statistics for each building category. From left to right: building category, total number of models, average/median/minimum/maximum number of mesh subgroups over the category's models (leaf nodes of the COLLADA metadata of the building models), average/median/minimum/maximum number of unique (non-duplicate) subgroups, average/median/minimum/maximum number of annotated unique mesh subgroups.

Category	num# models	avg# subgrps	med# subgrps	min# subgrps	max# subgrps	avg# un. subgrps	med# un. subgrps	min# un. subgrps	max# un. subgrps	avg# un. l.subgrps	med# un. l.subgrps	min# un. l.subgrps	max# un. l.subgrps
Residential	1,424	678.7	547	83	1989	167.1	144	61	920	61.4	50.0	7	613
Commercial	153	723.4	606	90	1981	159.8	139	70	907	49.4	44.0	3	223
Religious	540	487.0	348	93	1981	139.9	129	65	667	47.2	45.0	7	139
Civic	67	628.8	480	118	1822	144.4	123	75	618	43.0	43.0	8	106
Castles	85	609.8	485	125	1786	193.0	166	76	590	38.6	37	2	92
Whole Set	2,000	623.6	497.5	83	1989	160.5	140	61	920	55.9	47.0	2	613

Table 10: Statistics per building category regarding components (merged adjacent mesh subgroups). From left to right: building category, total number of models, average/median/minimum/maximum number of annotated components per model, average/median/minimum/maximum number of annotated unique (non-duplicate) components per model.

Category	num# models	avg# l.comp.	med# l.comp.	min# l.comp.	max# l.comp.	avg# un. l.comp.	med# un. l.comp.	min# un. l.comp.	max# un. l.comp.
Residential	1,424	321.8	243.0	13	1970	46.1	42.0	8	371
Commercial	153	408.0	296.0	4	1680	44.6	39.0	3	247
Religious	540	272.2	184.0	18	1469	37.7	35.0	6	135
Civic	67	378.4	263.0	36	1667	39.3	33.0	7	252
Castles	85	295.3	210.0	40	1200	30.5	28.0	2	107
Whole Set	2,000	316.6	231.0	4	1970	43.2	39.0	2	371

Table 11: BuildingGNN architecture: The Node representation combines the OBB - (Object Oriented Bounding Box) , SA - (Surface area), C - (centroid) and MN - (MinkowskiNet pre-trained features) for each sub group. The GNN is composed of (a) an encoder block made of three MLPs having 1, 3 and 5 hidden layers respectively, and (b) a decoder block with one MLP having 1 hidden layer followed by softmax. We refer to the code for more details.

	Layers	Output
Edge	(MLP(11×41, layer=1)))	41
Node	(6D(OBB)+1D(SA)+3D(C)+31D(MN)	41
Input	(Node$_i$ + Edge$_{ij}$ + Node$_j$)	41
Encoder	(MLP(Input×256, layer=1)))	64
	GN(LeakyReLU(0.2)))	64
	(MLP(64*3×128, layer=3)))	64
	GN(LeakyReLU(0.2)))	64
	(MLP(64*3×128, layer=5)))	64
	GN(LeakyReLU(0.2)))	64
Decoder	(MLP(128×64, layer=1)))	31
	softmax	31

The term results in zero cost for right angles between normals indicating a strong edge. The parameter λ is adjusted with grid search in the hold-out validation set.

Average vs max pooling. As discussed in our experiments section of our main paper, one possibility to aggregate probabilities of points associated per triangle or component is average pooling: $\mathbf{q}_t = \sum_{p \in P_t} \mathbf{q}_p / |P_t|$ where $\mathbf{q}_p$ and $\mathbf{q}_t$ are point and triangle probabilities respectively. An alternative is to use max pooling (i.e., replace sum with max above). We experimented with average vs max pooling also per component. As shown in Table 13, average pooling works better for both triangle- and component-based pooling (we experimented with MinkowskiNet per-point probabilities).

Table 12: Statistics for the number of BuildingGNN edges per type present in the graphs of the training buildings.

Label	max # edges	min # edges	mean # edges	# median edges
Proximity	16317	81	778.0	489.0
Similarity	762156	5	26452.1	4875.5
Containment	26354	71	2,054.5	1,390.0
Support	7234	7	687.5	492.0
All	772878	259	29972.1	7818.0

Experiments with different losses. We experimented with different losses for our MinkowskiNet variants for the "BuildingNet-Point" and "BuildingNet-Mesh" tracks. Specifically, we experimented with the Weighted Cross-Entropy Loss (WCE) described in our main paper, Cross-Entropy Loss (CE) without label weights, the Focal Loss (FL) [30], α-balanced Focal Loss (α-FL) [30], and Class-Balanced Cross Entropy Loss (CB) [10]. Table 14 and Table 15 show results for the "BuildingNet-Point" and "BuildingNet-Mesh" tracks respectively. We observe that

Table 13: "BuildingNet-Mesh" results using average and max pooling aggregation over triangles and components (weighted cross-entropy loss was used for all these experiments).

Method	Pool.	n?	c?	Part IoU	Shape IoU	Class acc.
MinkNet2Triangle	Avg	✓	×	**28.8%**	**26.7%**	**64.8%**
	Max	✓	×	28.6%	26.1%	64.4%
	Avg	✓	✓	**32.8%**	**29.2%**	**68.1%**
	Max	✓	✓	31.5%	28.1%	66.8%
MinkNet2Sub	Avg	✓	×	**33.1%**	**36.0%**	**69.9%**
	Max	✓	×	30.4%	32.4%	65.6%
	Avg	✓	✓	**37.0%**	**39.1%**	**73.2%**
	Max	✓	✓	32.7%	34.8%	67.4%

(a) in the case that color is not available, WCE is slightly better than alternatives according to all measures for both tracks (b) when color is available, CB is a bit better in terms of Part IoU, but worse in terms of Shape IoU than WCE in the case of the point cloud track. For the mesh track, CB is slightly better according to all measures. In general, WCE and CB behave the best on average, yet their difference is small. For the rest of our experiments, we use WCE.

Performance for each part label. Our main paper reports mean Part IoU performance in the experiments section. Table 18 reports the BuildingGNN-PointNet++ and BuildingGNN-MinkNet part IoU performance for each label. We also report the performance of MinkowskiNet and PointNet++ for the point cloud track. We observe that networks do better for common part labels, such as window, wall, roof, plant, vehicle, while the performance degrades for rare parts (e.g., awning, arch), or parts whose shape can easily be confused with other more dominant parts (e.g., garage is often confused with door, wall, or window).

Table 14: "BuildingNet-Point" track results using the Weighted Cross-Entropy Loss (WCE), Cross-Entropy Loss (CE), Focal Loss (FL), α-balanced Focal Loss (α-FL) and finally Class-Balanced Cross Entropy Loss (CB). All these were used to train the MinkowskiUNet34 architecture. For the FL and α-FL experiments the γ hyper-parameter was set to 2.0 and for the α-FL the same weights were used as the weighted cross entropy loss (see Section 4.3 in our main paper). For the CB experiments we set $\beta = 0.999999$.

Method	Loss	n?	c?	Part IoU	Shape IoU	Class acc.
MinkNet	WCE	✓	×	**26.9%**	**22.2%**	**62.2%**
	CE	✓	×	24.5%	21.2%	61.3%
	FL	✓	×	26.1%	21.8%	61.2%
	α-FL	✓	×	22.3%	19.8%	61.5%
	CB	✓	×	26.4%	20.9%	61.4%
MinkNet	WCE	✓	✓	29.9%	24.3%	**65.5%**
	CE	✓	✓	28.5%	24.5%	65.3%
	FL	✓	✓	28.7%	24.9%	65.2%
	α-FL	✓	✓	30.1%	**25.3%**	65.2%
	CB	✓	✓	**30.4%**	24.0%	**65.5%**

Table 15: "BuildingNet-Mesh" results using different loss functions

Method	Loss	n?	c?	Part IoU	Shape IoU	Class acc.
MinkNet2Sub	WCE	✓	×	**33.1%**	**36.0%**	**69.9%**
	CE	✓	×	30.7%	32.7%	68.8%
	FL	✓	×	31.0%	33.4%	67.9%
	α-FL	✓	×	27.2%	28.3%	66.7%
	CB	✓	×	32.9%	34.3%	69.1%
MinkNet2Sub	WCE	✓	✓	37.0%	39.1%	73.2%
	CE	✓	✓	35.6%	39.2%	73.5%
	FL	✓	✓	35.1%	38.4%	73.2%
	α-FL	✓	✓	36.0%	38.2%	72.4%
	CB	✓	✓	**38.0%**	**39.7%**	**73.9%**

Table 16: BuildingGNN ablation study based on PointNet++ node features

Variant	n?	c?	Part IoU	Shape IoU	Class acc.
Node-OBB	✓	✓	10.0%	17.1%	56.5%
Node-PointNet++	✓	✓	14.0%	19.1%	52.2%
Node-OBB+PointNet++	✓	✓	24.4%	27.8%	71.7%
w/ support edges	✓	✓	26.7%	29.2%	71.5%
w/ containment edges	✓	✓	27.9%	30.6%	72.6%
w/ proximity edges	✓	✓	26.4%	29.4%	71.4%
w/ similarity edges	✓	✓	23.1%	28.5%	69.8%
BuildingGNN-PointNet++	✓	✓	**31.5%**	**35.9%**	**73.9%**

Table 17: BuildingGNN ablation study based on MinkowskiNet node features

Variant	n?	c?	Part IoU	Shape IoU	Class acc.
Node-OBB	✓	✓	10.0%	17.1%	56.5%
Node-MinkNet	✓	✓	35.6%	35.9%	67.7%
Node-OBB+MinkNet	✓	✓	40.0%	40.6%	75.8%
w/ support edges	✓	✓	42.0%	43.5%	77.8%
w/ containment edges	✓	✓	41.1%	42.0%	76.8%
w/ proximity edges	✓	✓	39.9%	40.6%	75.6%
w/ similarity edges	✓	✓	41.2%	43.0%	75.8%
BuildingGNN-MinkNet	✓	✓	**42.6%**	**46.8%**	**77.8%**

Appendix E: BuildingGNN ablation study

We conducted an ablation study involving different node features, and also experimenting with different types of edges in our BuildingGNN. Table 16 present the results for different experimental conditions of our BuildingGNN based on PointNet++ as node features. We first experimented using no edges and processing node features alone through our MLP structure. We experimented with using only OBB-based features ("Node-OBB"), using features from PointNet++ alone ("Node-PointNet++"), and finally using both node features concatenated ("Node-OBB+PointNet++"). We observe that using all combinations of node features yields better performance compared to using either node feature type alone. Then we started experimented with adding each type of edges individually to our network (e.g., "w/ support edges" in Table 16 means that we use node features with support edges only). Adding

Table 18: Part IOU performance for each label. BuildingGNN-MinkNet and BuildingGNN-PointNet++ are tested on the mesh track, while MinkNet and PointNet++ are tested on the point cloud track. The left half of the table reports performance when color is available ("n+c"), while the right half reports performance when it is not available ("n").

Label	BuildingGNN MinkNet(n+c)	BuildingGNN PointNet++(n+c)	MinkNet (n+c)	PointNet++ (n+c)	BuildingGNN MinkNet(n)	BuildingGNN PointNet++(n)	MinkNet (n)	PointNet++ (n)
Window	70.5%	71.1%	44.1%	34.8%	70.4%	68.3%	35.6%	0.0%
Plant	81.0%	69.8%	79.6%	70.3%	79.8%	69.8%	79.7%	48.4%
Vehicle	83.7%	77.3%	77.1%	29.7%	82.7%	72.4%	75.8%	19.2%
Wall	78.1%	77.5%	64.5%	57.9%	76.0%	74.4%	63.2%	54.4%
Banister	50.0%	19.9%	44.9%	0.0%	56.5%	22.0%	45.6%	0.0%
Furniture	59.7%	37.0%	56.0%	0.0%	58.3%	43.5%	54.9%	0.0%
Fence	55.5%	34.7%	71.3%	16.5%	64.1%	19.7%	49.5%	9.6%
Roof	78.9%	72.1%	65.3%	58.2%	70.2%	69.0%	67.0%	56.4%
Door	41.7%	37.6%	21.7%	0.0%	39.2%	37.7%	23.8%	0.0%
Tower	53.4%	41.2%	46.5%	2.3%	50.8%	37.5%	43.4%	4.8%
Column	61.5%	27.6%	49.5%	0.6%	53.6%	34.7%	42.9%	1.1%
Beam	24.9%	22.4%	13.8%	0.02%	30.3%	21.5%	17.2%	0.0%
Stairs	38.6%	25.6%	26.9%	0.0%	41.0%	24.1%	27.8%	0.0%
Shutters	1.0%	1.3%	0.0%	0.0%	1.7%	0.0%	0.0%	0.0%
Garage	9.0%	10.6%	3.6%	0.0%	10.6%	8.4%	6.8%	0.0%
Parapet	24.9%	3.9%	11.6%	0.0%	28.6%	2.5%	21.0%	0.0%
Gate	14.0%	16.5%	6.4%	0.0%	7.9%	12.3%	7.9%	0.0%
Dome	53.8%	10.1%	48.0%	1.9%	54.3%	14.2%	54.5%	16.3%
Floor	51.5%	37.7%	47.8%	36.9%	51.2%	30.9%	46.8%	30.0%
Ground	75.0%	65.1%	77.4%	64.1%	61.8%	55.5%	60.8%	42.6%
Buttress	23.8%	9.6%	15.6%	0.0%	38.7%	12.3%	6.1%	0.0%
Balcony	19.6%	9.5%	15.0%	0.0%	15.5%	15.6%	17.3%	0.0%
Chimney	70.0%	50.9%	57.9%	0.0%	53.6%	49.5%	60.1%	0.0%
Lighting	6.4%	9.1%	16.8%	0.0%	24.9%	3.5%	23.3%	0.0%
Corridor	16.3%	10.5%	15.9%	4.2%	7.2%	4.1%	7.2%	0.0%
Ceiling	28.0%	23.8%	22.1%	4.6%	28.0%	20.5%	17.4%	4.6%
Pool	70.8%	53.0%	78.7%	77.8%	38.1%	33.0%	43.0%	0.0%
Dormer	27.3%	20.4%	9.6%	0.0%	22.1%	23.3%	6.8%	0.0%
Road	46.2%	24.1%	53.5%	40.0%	1.9%	16.3%	21.5%	0.0%
Arch	8.4%	5.2%	0.9%	0.0%	3.2%	2.9%	0.8%	0.0%
Awning	1.5%	0%	3.8%	0.0%	1.6%	0.0%	0.0%	0.0%

each type of edge individually further boosts performance compared to using node features alone. Using all edges ("BuildingGNN-PointNet") yields a noticeable 7.1% Part IoU increase and 8.1% Shape IoU increase compared to using node features alone. Table 17 shows the same experiments using MinkowskiNet-based features. We observe that combined node features perform better than using either node feature type alone. Adding each type of edges helps, except for proximity edges that seem to have no improvement when used alone. Using all edges still yields a noticeable 2.6% Part IoU increase and 6.2% Shape IoU increase compared to using node features alone.

We also experimented with DGCNN [57] as a backbone in our GNN for extracting node features. Unfortunately, DGCNN could not directly handle our large points clouds (100K points). It runs out of memory even with batch size 1 on a 48GB GPU card. We tried to downsample the point clouds (10K points) to pass them to DGCNN, then propagated the node features back to the 100K points using n-earest neighbor upsampling. The part IoU was 32.5% in the mesh track with color input and using all edges (i.e., the performance is comparable to BuildingGNN-PointNet++, but much lower than BuildingGNN-MinkNet). Still, since other methods were able to handle the original resolution without downsampling, this comparison is not necessarily fair, thus we excluded it from the tables showing the track results in our main paper.

Appendix F: Additional Material

As additional supplementary material of our paper, we include part of our video tutorial that demonstrates our UI functionality (see MP4 video in the supplementary zip file). Finally, we refer readers to our project page `www.buildingnet.org` for the dataset and source code.